LES validation of urban flow, part I: flow statistics and frequency distributions

Article

Accepted Version

Hertwig, D., Patnaik, G. and Leitl, B. (2017) LES validation of urban flow, part I: flow statistics and frequency distributions. Environmental Fluid Mechanics, 17 (3). pp. 521-550. ISSN 1567-7419 doi: https://doi.org/10.1007/s10652-016-9507-7 Available at http://centaur.reading.ac.uk/76907/

Environ Fluid Mech manuscript No.
(will be inserted by the editor)

LES validation of urban flow, part I: flow statistics and frequency distributions

Denise Hertwig · Gopal Patnaik · Bernd Leitl

Received: date / Accepted: date

Abstract Essential prerequisites for a thorough model evaluation are the availability of problem-specific, quality-controlled reference data and the use of model-specific comparison methods. The work presented here is motivated by the striking lack of proportion between the increasing use of large-eddy simulation (LES) as a standard technique in micrometeorology and wind engineering and the level of scrutiny that is commonly applied to assess the quality of results obtained. We propose and apply an in-depth, multi-level validation concept that is specifically targeted at the time-dependency of mechanically induced shear-layer turbulence. Near-surface isothermal turbulent flow in a densely built-up city serves as the test scenario for the approach. High-resolution LES data are evaluated based on a comprehensive database of boundary-layer wind-tunnel measurements.

From an exploratory data analysis of mean flow and turbulence statistics, a high level of agreement between simulation and experiment is apparent. Inspecting frequency distributions of the underlying instantaneous data proves to be necessary for a more rigorous assessment of the overall prediction quality. From velocity histograms local accuracy limi-

D. Hertwig
Meteorological Institute, University of Hamburg
Bundesstrasse 55, D-20146 Hamburg, Germany
Present address:
Department of Meteorology, University of Reading
P.O. Box 243, Reading, RG6 6BB, UK
E-mail: d.hertwig@reading.ac.uk
Tel.: +44-118-378-6721
Fax: +44-118-378-8905

G. Patnaik
Laboratories for Computational Physics and Fluid Dynamics
U.S. Naval Research Laboratory
Washington D.C., USA
E-mail: gopal.patnaik@nrl.navy.mil

B. Leitl
Meteorological Institute, University of Hamburg
Bundesstrasse 55, D-20146 Hamburg, Germany
E-mail: bernd.leitl@uni-hamburg.de

tations due to a comparatively coarse building representation as well as particular strengths of the model to capture complex urban flow features with sufficient accuracy are readily determined. However, the analysis shows that further crucial information about the physical validity of the LES needs to be obtained through the comparison of eddy statistics, which is focused on in part II.

Compared with methods that rely on single figures of merit, the multi-level validation strategy presented here supports conclusions about the simulation quality and the model's fitness for its intended range of application through a deeper understanding of the unsteady structure of the flow.

Keywords Large-eddy simulation · Model validation · Quality assurance · Turbulent flow · Urban environment · Wind tunnel

1 Introduction

Unsteady flow in built environments is an important representative of the complex nature of near-surface atmospheric turbulence. Studying and characterising urban flow fields is of strong practical interest with regard to issues like urban ventilation and pollutant dispersion, wind and thermal comfort, heat and moisture transfer and other urban micro-climatic processes [17,32,60,42,43]. Such problems cannot easily be investigated by means of classic *in-situ* measurements, making high-resolution computational fluid dynamics (CFD) simulations increasingly attractive for wind engineering and micro-meteorological communities [45,34,61,62].

Obstacle-resolving micro-scale meteorological models based on the Reynolds-averaged Navier-Stokes (RANS) equations are routinely applied to investigate urban flow and dispersion phenomena, e.g. [27,65]. Rapid advancements in computer capacities over the last 15 years or so, however, have increased the use of turbulence-resolving numerical approaches like large-eddy simulation (LES) for similar applications on the urban scale [61]. In contrast to RANS simulations, eddy-resolving approaches have the potential to adequately reproduce complex turbulent flow regimes together with their temporal evolution [30].

Comparative studies have revealed advantages of urban LES over steady-state RANS approaches on the mean-flow level. Xie and Castro [72] for example compared LES and RANS predictions of flow over a cube array to wind-tunnel measurements and data from direct numerical simulation. While the accuracy of RANS was found to be comparable to LES well above the urban canopy layer (UCL), it deteriorates below rooftop. The better performance of LES in the UCL was attributed to the ability to capture unsteady urban flow features. Similar conclusions were drawn by Salim et al. [54] for pollutant dispersion in a street canyon and by Tominaga and Stathopoulos [63,64], who compared RANS and LES dispersion fields within an isolated street and a cube array. In both configurations, the LES results were in better agreement with the reference experiments and provided a more realistic picture of the characteristics of the pollutant plume.

Most of today's published studies on urban LES were conducted in strongly idealised urban environments (e.g. isolated buildings, isolated street canyons, idealised building arrays). However, in recent years the complexity of the flow problems being analysed has increased. LES studies of flow and dispersion in realistic urban settings and in larger domains, extending into neighbourhood and city scales are now available as well [51,73,41]. Other studies have focused on advancing the level of physical complexity covered by the simulations, e.g. by representing atmospheric stability effects [74], differential heating of urban surfaces [19, 49,38,39] or aerodynamic effects of urban greenery [44].

The focus of the work presented here is put on how the quality of such turbulence-resolving simulations can be assessed and quantified by taking into account the time-dependent nature of the model output.

A thorough validation of the model is a crucial step in establishing confidence in its skill and reliability and to assess possible bounds of uncertainty for cases in which the truth is not known *a priori*. The first important step for validating numerical models is finding reliable, reproducible reference data that provide detailed information about important flow parameters, against which the model performance and uncertainty can be assessed. Due to the increase of information about unsteady flow dynamics available from LES there is an increasing demand on the overall quantity of reference data and the level of detail about the flow that can be derived from such data [2, 35]. In order to avoid incorrectly accepting the time-resolved model results as the "ground truth" [71], strategies pursued in LES validation have to provide information of whether the simulation adequately reproduces the spatial-temporal behaviour of turbulent eddies in the flow. While validation standards for RANS-type simulations have been defined in the past [67, 15, 16, 55], as of now there has been no similar community-wide effort leading to similar consensus about standards for an in-depth validation of LES.

Since the non-linear nature of turbulence precludes the direct comparison of instantaneous fields or time series from experiment and LES, the validation has to rely on statistical approaches. As commonly done with RANS results, comparisons between LES and experiments typically concentrate only on low-order statistics like means, variances or co-variances. However, the evaluation of turbulence-resolving simulations should also assess to what degree the model is able to reproduce the structure of turbulence. For this purpose, it is important to compare higher-order turbulence parameters such as e.g. integral time scales, spectral energy, and the scales of motions contributing to turbulent fluxes, which can be determined using time-series analysis methods.

With this study we propose a multi-level LES validation concept for turbulent flow in the near-surface atmospheric boundary layer. Instead of relying on single figures of merit, the validation concept focuses on the comparative analysis of a multitude of relevant flow quantities. By focusing on eddy statistics and characteristics of turbulence structures in simulation and experiment, the procedure specifically aims at the heart of LES: the representation of energy-containing eddies. We test the suitability of the proposed validation strategy based on flow in a complex urban environment: the high-density urban centre of the city of Hamburg, Germany. Turbulent flow is simulated with a high-resolution eddy-resolving aerodynamics code based on an implicit LES approach. With respect to resolution, domain size, and computing times, the code represents the advanced state-of-the-art. Reference data are available from boundary-layer wind-tunnel measurements in an urban scale model.

In part I of this study, presented in the following, we are introducing the validation concept (Sect. 2) and present an overview of the test case together with specifics of the LES and the wind-tunnel experiment (Sect. 3). We also cover the first level of the proposed validation strategy, the exploratory data analysis. This step focuses on comparing mean flow and turbulence statistics (Sect. 4) and the underlying frequency distributions of instantaneous velocities in the horizontal plane (Sect. 5). Initial conclusions drawn from this first comparisons are discussed in Sect. 6.

In part II we extend the validation exercise to the comparison of turbulence scales by means of temporal auto-correlations and turbulence spectra and discuss comparisons based on the applications of conditional resampling (quadrant analysis) and joint time frequency analyses (wavelet transform).

2 Validation method

At the start of the computer revolution in fluid mechanics, Bradshaw [14] predicted a "fact gap" emerging between the capability to simulate turbulent flow in unprecedented detail and the potential to determine the accuracy of such simulations with experiments. As discussed by Oberkampf and Trucano [47], numerical and experimental approaches in engineering historically had a tendency of being competitive rather than complementary, resulting in CFD proceeding "(...) on a path that is largely independent of validation". Similarly, Wyngaard and Peltier [71] stated that the coupling between experiments and modelling that has a strong tradition in micro-meteorology has been remarkably lacking in meteorological LES.

A model is validated in order to determine whether its combination of conceptual and computational components allow an accurate simulation of the physical problem of interest from the perspective of a specific application [1,25,47]. Model validation primarily depends on two essential factors: the availability of suitable reference data [37] and the application of comparison strategies for model-specific performance assessments [57,47,4]. Whether or not reference data are suitable strongly depends on the level of description provided by the simulation. For turbulence-resolving CFD techniques like LES, the experimental design should be suitable for the characterisation of flow structures. In an ideal scenario, the quantities of interest are provided with a spatial-temporal resolution that is comparable to that of the numerical output [2]. Presently, time-resolved single-point measurements and space-resolved multi-point (mostly 1D or 2D) fields of either low time resolution or restricted spatial extent represent the state-of-the-art of experiments in the field and laboratory. In the case of urban flow, using space-resolving measurement techniques like laser-based particle image velocimetry in the wind tunnel is a challenge as not all desired locations may be accessible deep within street canyons.

We propose a multi-level concept for the in-depth LES validation for turbulent flow in the near-surface boundary-layer based on experimental data, which is schematically illustrated in Fig. 1. At the "data level" we consider instantaneous, time-resolved LES flow quantities, e.g. in terms of the instantaneous velocity components $U_i^{les}(\mathbf{x},t)$, with $i = 1,2,3$, which depend on the filter width Δ_i, the mesh size h_i, and the time resolution δt, as well as their experimentally resolved instantaneous counterparts, $U_i^{exp}(\mathbf{x},t)$, with space and time resolutions, δx_i and δt, that are provided by the respective measurement technique. As an important prerequisite for a fair performance assessment the model validation should be performed as a blind test; neither the measurements nor the simulation should be deliberately tuned to optimise the level of agreement. This means that data exchange before running the model should be restricted to information about relevant boundary conditions of the experiment, enabling modellers to limit the degrees of freedom in the simulation setup.

The "testing level" is divided into three parts, starting with an initial exploratory data analysis through the comparison of low-order statistics. This general assessment can then be further supported by analysing the frequency distributions of the underlying instantaneous flow variables. This enables more wide-ranging conclusions to be drawn about the overall agreement of sample characteristics. Since LES directly resolves the energy-carrying eddies of the flow, the second level focuses on a comparative analysis of eddy statistics. Based on multi-point and/or multi-time correlations, integral length/time scales as well as spatial/temporal structure functions can be derived and compared. Further insights into the structure of turbulence can also be gained from the comparison of energy-density spectra. In the third and final level of the validation, advanced methods from the field of flow pattern recognition are applied in order to evaluate the representation of eddy structures based on their scale statistics. Depending on the resolution properties of the data, established ap-

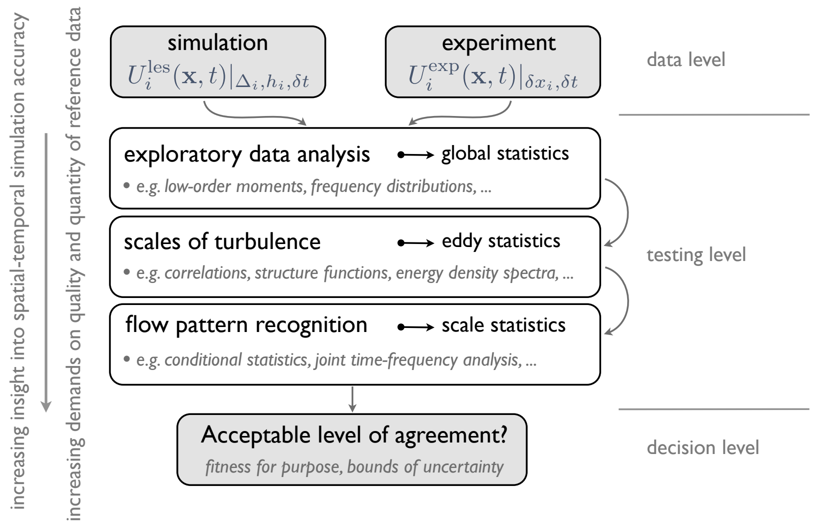

Fig. 1: Hierarchy of analysis methods for LES validation of turbulent boundary layer flow.

proaches based on conditional resampling (e.g. as part of quadrant analysis of turbulent fluxes), joint time-frequency analyses (e.g. using wavelet transform methods), or flow reconstruction techniques, e.g. by means of empirical orthogonal functions or stochastic estimation [31], can be employed here.

Based on the outcome of these comparisons, in the final "decision level" it has to be decided whether or not the level of agreement between simulation and reference data is sufficient and hence if the model is acceptable for its intended application. If the answer is negative, the findings from the testing level should be used to determine necessary improvements to the model and the testing has to be repeated until the desired level of agreement is achieved. Whether or not the simulation quality is deemed sufficient and what deviations from the experiment are considered acceptable, strongly depends on the intended use of the model and possible consequences related to the margins of uncertainty of the simulation. In validation studies of steady-state CFD-RANS models it is common practice to base the decision about the quality of the model on one-dimensional statistical measures known as validation metrics, e.g. [16]. By defining acceptable, application-specific thresholds for these metrics the model performance can be judged and easily compared with other models. This approach can be employed as part of the exploratory data analysis proposed above. However, validation metrics do not offer direct physical insight and inferring information about reasons for accuracy limitations is difficult. Therefore it is generally recommended to use these measures in combination with detailed point-by-point analyses. Such detailed comparisons can for example focus on questions like: *Are space/time patterns or trends in the variables of interest reproduced by the LES? Are flow features captured that are important for the problem under study? Do general conclusions about the physical state of the flow in the LES agree with the experiment?* In practice the corresponding qualitative and quantitative information can for example be based on height profiles of the variables of interest, on comparisons of histograms or of time-lag or frequency dependent statistics. The

LES results from the validation test case presented in the following will be assessed along these lines.

3 Test case, experiment and simulation

The validation method is applied to the case of isothermal urban flow in the city of Hamburg, Germany, for which high-resolution LES data and comprehensive boundary-layer wind-tunnel data were generated. Fig. 2 shows the regions covered by the computational and experimental domains, respectively. Information about the urban test environment, the laboratory experiment and the LES are presented in the following sections.

3.1 Urban test environment

The domain of interest is centered on the inner city area of Hamburg. The Elbe river separates the industrial harbour area to the south, mainly featuring low-story storage buildings and production facilities, from the inner-city district to the north that is characterised by high-rise, high-density building structure. The urban morphology of the inner city corresponds to typical northern and central European cities with closely packed, heterogeneously shaped buildings of similar heights, narrow street canyons and complex intersections. Based on the buildings included in the wind-tunnel domain, an average building height of $H = 34.3$ m is obtained for the district north of the Elbe. Here, typical street canyon widths are in the order of $W = 20$ m, with individual street widths between 10 m and 50 m. The typical street-canyon aspect ratio in the inner city is $H/W = 1.72$, with individual values ranging between 0.7 and > 3. This implies the dominance of skimming flow regimes, while in the presence of open spaces or wide intersections chaotic wake-interference flow is prevailing [24,40]. In the industrial area on the southern shore of the river, the average building height is much lower with an average of about 21 m and isolated roughness flow is prevailing.

3.1.1 Flow comparison sites

Overall 22 sites distributed across the inner city were selected for the validation exercise in order to cover a wide range of typical UCL flow features and investigate the influence of changes in the underlying city structure on roughness-sublayer flow. Data are mostly available in terms of densely spaced vertical profiles, allowing the investigation of the height-dependent structure of the flow and vertical momentum exchange. Fig. 3 shows the positions of the flow comparison sites. Locations marked by the prefix “BL” are distributed at various downstream positions within the gradually increasing internal boundary layer forming after the roughness change from the industrial harbour region to the inner city, which are separated by the Elbe river. The “RM” locations are closely distributed around the city hall. This area is interesting due to its diverse building geometry. Within the “DM” area, reference measurements were carried out with a higher horizontal resolution in order to resolve the flow field at a courtyard entrance. Based on this sample of comparison sites it is possible to assess whether the LES is able to capture important flow features like wake recirculation in cross-wind canyons (BL11), helical motions in canyons oriented at oblique angles (BL12), flow channelling in along-wind canyons (RM07), flow through geometrically confined open spaces (e.g. BL08, BL10, RM10, RM09), intersection flow (RM03, BL10), stagnating flow

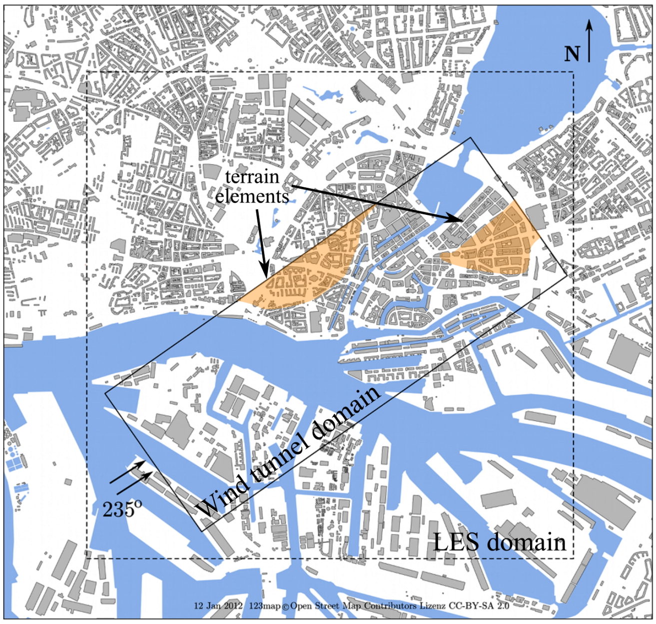

Fig. 2: Experimental and computational domains covering the inner city of Hamburg. Solid rectangle: 1.4 km × 3.7 km wind-tunnel model area; dashed square: 4 km × 4 km computational domain for the LES. The areas in which terrain is relevant and therefore included in the wind-tunnel scale model are indicated as well. The maximum offsets to ground level are 20 m (terrain to the west) and 7 m (terrain to the east).

on the windward side of a building (BL07) and flow into and within courtyards (DM, BL09). Capturing such flow features is essential for an accurate simulation of scalar dispersion in cities regarding both the mean plume structure and local, time-dependent concentration fluctuations. The unobstructed site BL04 above the Elbe river is representative of the approach flow conditions upstream of city centre in LES and experiment and used as a flow reference location (see Sect. 3.2.2).

3.2 Wind-tunnel experiment

Flow experiments were conducted in the open-circuit boundary-layer wind tunnel WOTAN of the Environmental Wind Tunnel Laboratory (EWTL) at the University of Hamburg. With a test section of 18 m in length, 4 m in width and a ceiling of adjustable height between 2.75 m and 3.25 m, WOTAN is one of the largest low-speed, suction-type wind tunnel facilities worldwide for the physical modelling of isothermal boundary layers.

Information about buildings, terrain elevations and outlines of bodies of water in central Hamburg was provided by the Hamburg geo-information service. Detailed 3D building data was available at a minimum resolution of 0.5 m. The wind-tunnel model was built at a scale of 1:350, reproducing all relevant buildings down to 0.5 m full scale (approx. 1.5 mm in model scale). The longitudinal/lateral extents of the model area were 3.7 km/1.4 km full-scale (10.5 m/4 m model scale). Rolling terrain was reproduced by stacking layers of thin

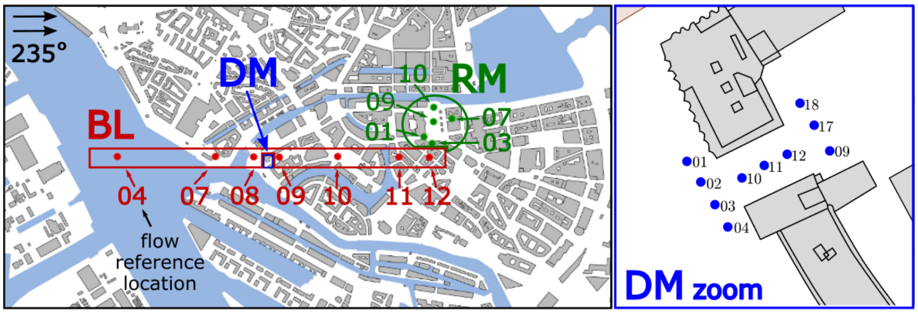

Fig. 3: Left: wind-tunnel model area indicating locations and IDs of the flow comparison sites: boundary-layer development positions (prefix BL, red dots), sites around the city hall (prefix RM, green dots), and the dense measurement site at a courtyard entrance (DM, blue rectangle). Right: exact locations of the 10 DM sites.

wooden plates, each having a depth of 2 mm in model scale equating to offsets of 0.7 m in the field (areas indicated in Fig. 2). The water level of the Elbe river and city canals was represented as being close to high tide, resulting in a full-scale vertical offset of 3.5 m to land (1 cm in model scale). The most significant abstraction of the scale model is given by neglecting all types of urban vegetation, smaller bridges and traffic overpasses. The model orientation with the ambient flow approaching from the south-west (235°) represents a predominant meteorological situation for the city. Fig. 4 shows the inner city area as viewed from 235° (south-west) and 35° (north-east) together with corresponding views in the laboratory.

3.2.1 Inflow specifications and modelling

Properly chosen flow boundary conditions in the reference experiment are vital for model validation. Specifying appropriate inflow boundary conditions is not a trivial task, especially when investigating flow in urban areas.

As a guidance for the generation of realistic inflow conditions for both the wind-tunnel model and the LES, information about vertical mean flow and turbulence profiles were derived from meteorological tower measurements [68]. The tower is situated in a suburban setting about 8 km south-east of the study domain. *In-situ* sonic anemometer measurements of all three velocity components and temperature were available at five measurement heights (10 m, 50 m, 110 m, 175 m and 250 m) at resolutions of 10 and 20 Hz. Detailed information about the facility and local climatology are presented by Konow [36]. An in-depth description of the field data analysis for the validation test case is presented by Hertwig [29]. For the sake of brevity only the main findings are summarised here.

Based on a three year data record (2007–2009) the roughness length z_0 and the power-law wind profile exponent α were derived for flow approaching the tower from a sector of $235° \pm 30°$ under neutral stability conditions. Within this sector, the surface roughness characteristics are very homogeneous with mixed land use and low-density industrial zones, frequently loosened by side branches of the Elbe river. Structurally this is comparable to the situation in the inflow corridor for the wind-tunnel model, although the latter is expected to be rougher due to the harbour industry. z_0 was found to be of order $1.2\ \text{m} \pm 0.24\ \text{m}$, whereas α was 0.29 ± 0.01 based on a reference height of 175 m. This reference height was found to

Fig. 4: Aerial photographs of the central part of the Hamburg domain together with the representation in the wind-tunnel model. Left: view from the south-west towards the inner city area. Right: view from the north-east towards the industrial harbour.

be representative of the depth of the surface layer (constant flux layer) for neutral stability conditions and mean wind speeds higher than 1 m s^{-1}. For the derivation of turbulence intensities, spectral energy densities, and integral length scales the data was analysed over periods of negligible synoptic trends.

These characteristics were used as benchmarks for the physical modelling process in the wind tunnel. In addition, the generated laboratory boundary layer characteristics were in agreement with wind-tunnel modelling guidelines and established standards, e.g. [23, 66]. At the tunnel entrance an array of 7 flat vortex generators with triangular front faces was mounted (modified Standen spires [59]). The subsequent 7.2 m long flow development section was covered with 25 rows of floor roughness elements (sharp-edged metal brackets) arranged in a staggered array to generate realistic suburban/urban roughness conditions. It was experimentally verified that stationary and horizontally homogeneous flow conditions were established at the end of the development section just upstream of the urban model.

Fig. 5 shows that vertical profiles of mean streamwise velocities, turbulence intensities and turbulence integral length scales derived from the field measurements and the wind-tunnel approach flow are in good agreement. Overall the wind tunnel approach flow corresponds to a rougher surface type ($z_{0_{WT}} = 2\ \mathrm{m} \pm 0.67$ m with $\alpha_{WT} = 0.29 \pm 0.01$). This trend is also seen in the turbulence intensities based on the spanwise and vertical velocity components (not shown). The rougher surface characteristics of the wind-tunnel flow are expected to better represent the actual flow situation in the presence of the industrial harbour, which starts approximately 4 km upstream of the domain inflow edge. This feature is not seen by the field site sensors for the same south-westerly approach flow direction.

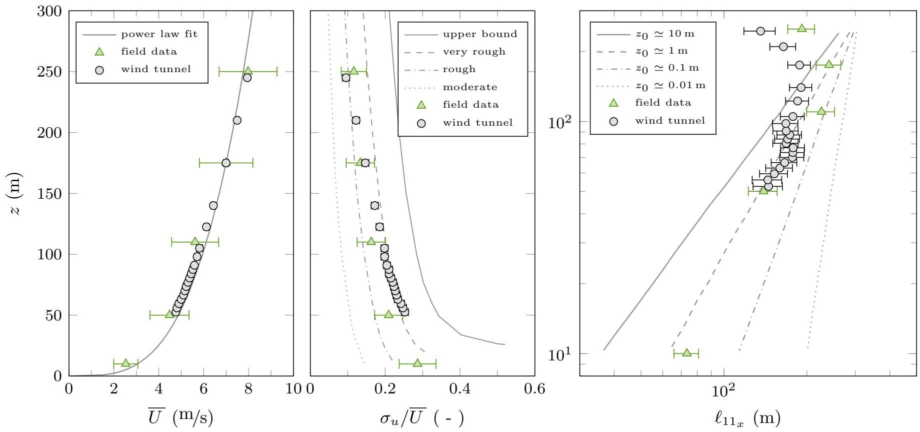

Fig. 5: Comparison of field (triangles) and wind tunnel (dots) vertical profiles in the approach flow boundary layer. Left: mean streamwise velocity together with a power-law fit for $\alpha = 0.29$. Centre: turbulence intensity of the streamwise velocity with empirical boundaries for different roughness regimes according to ESDU [23]. Right: turbulence integral length scales in longitudinal direction derived from streamwise velocities. Lines indicate empirical boundaries of different roughness regimes following Counihan [20].

3.2.2 Flow measurements

Schematics of the wind tunnel model area and of the flow measurement set-up are presented in Fig. 6. The free-stream velocity was $U_\infty \simeq 10$ m s^{-1} to ensure Reynolds number independence. This was tested over a wide range of velocities, with the selected U_∞ being on the safe side even when measuring in narrow urban street canyons. In order to guarantee *Re*-independence close to solid boundaries, model buildings and ground plates all had aerodynamically rough surfaces. The characteristic flow Reynolds number in the test section was $Re \simeq 2.67 \cdot 10^6$ based on U_∞ and a length scale of 4 m (tunnel width). Within the urban scale model this corresponds to $Re_H = 2.97 \cdot 10^4$ based on the average inner city building height H and a typical velocity at this height of $U_H \simeq 4.55$ m s^{-1}, which was determined at the end of the flow development section. Re_H complies well with established criteria for the reliable physical modelling of urban flows, as outlined for example by Plate [52]. The wind-tunnel measurement sites shown in Fig. 3 where located in sufficient distance to lateral and outflow boundaries of the tunnel to ensure that the local flow field at these sites is neither affected by boundary layers forming at the tunnel side-walls or by the open outflow at the end of the test section.

Single-point high-resolution velocity records were acquired with a two-component fibre-optic Dantec laser Doppler anemometry (LDA) system. The LDA was operated to simultaneously measure the streamwise and vertical velocities (U–W mode) and the streamwise and spanwise velocities (U–V mode) using laser beams with wavelengths of 514.5 nm and 488 nm. With a focal length of 160 mm and an initial beam separation of 15 mm the LDA measuring volume had a diameter of 0.08 mm and a length of 1.6 mm. Haze-droplets with diameters of 1–2 μm emitted by a commercial-grade hazer were used to seed the flow. The LDA probe was moved by an automated 3D traverse system. The average LDA sampling frequencies (mean data rates $\dot{N}$) depend on local seeding conditions within the model do-

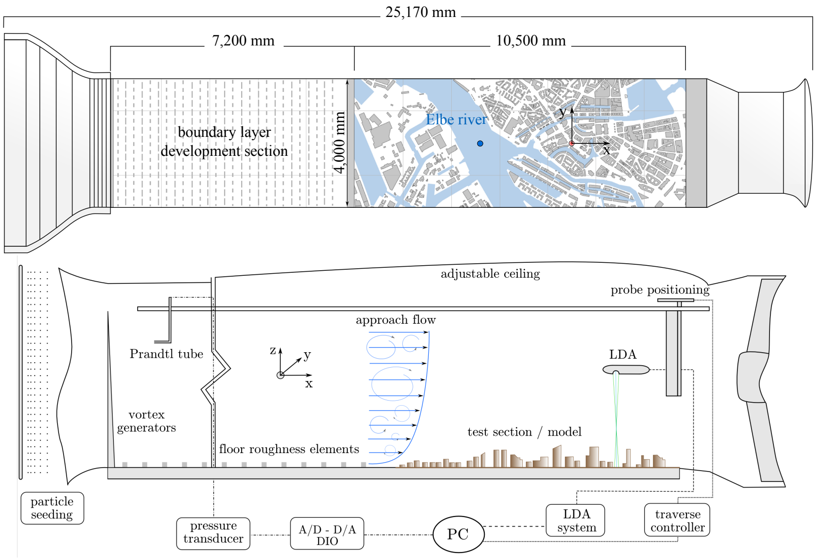

Fig. 6: Top: plan-view of the boundary-layer wind tunnel WOTAN. The red dot marks the coordinate origin and the flow reference location above the Elbe river is indicated by the blue dot. Bottom: side-view of the measurement set-up with the LDA probe aligned in U–V mode. Note that distances and heights are not true to scale. The flow is approaching from the left.

main and were typically in the order of 50 Hz (locations with low wind speeds) to 600 Hz (high wind speeds). Time series were recorded for 170 s to minimise the inherent uncertainty in derived statistics and enable representative analyses of large eddy structures. The measurement duration was determined from statistical convergence tests conducted at various flow locations. Taking into account the geometric scale of 1:350 this corresponds to a full-scale measurement duration of about 16.5 h at the same reference velocity.

A pitot-static tube was operated together with the LDA to record the free-stream velocity U_∞ in the tunnel during each measurement run. The pitot-tube signal was recorded by a pressure transducer delivering voltage signals to an analog-to-digital converter. All LDA-measured velocities and derived quantities are referenced to U_{ref} corresponding to the mean streamwise velocity at a height of $z_{ref} = 49$ m above the Elbe river (i.e. 45.5m or 1.33H above ground level; see Fig. 6).

3.2.3 LDA signal resampling

By nature, LDA provides discontinuous flow information. The time step between detected velocity signals is not uniform since seeding particles pass the measuring volume at random intervals. For time-series analyses in this study, the discontinuous time records are resampled to a new constant time step δt_r given by the inverse of the mean data rate $\dot{N}$. We reconstruct the LDA signals by using a 0th order polynomial interpolation, known in signal-processing as sample-and-hold technique (S&H) [22].

Fig. 7 shows frequency distributions of streamwise velocity fluctuations obtained from the raw LDA data and the corresponding S&H signal interpolation together with results

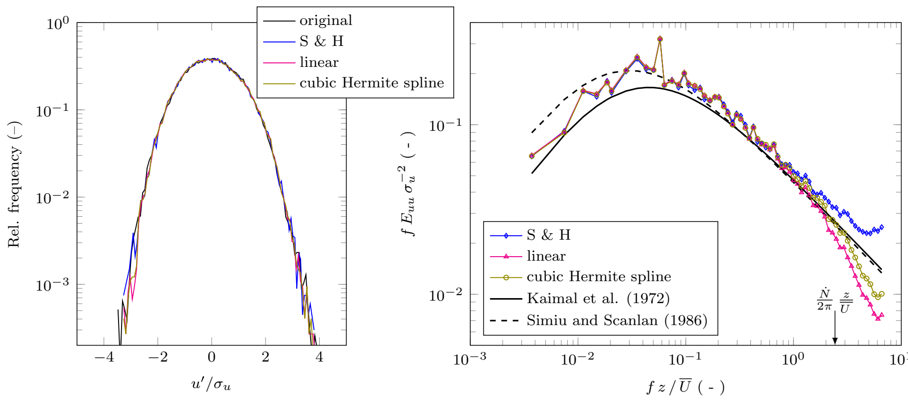

Fig. 7: Quality assessment of reconstructed LDA signals based on an example time series taken at a full-scale height of $z = 45.5$ m with a mean data rate of $\dot{N} = 551$ Hz. Left: normalised frequency distributions of the streamwise velocity fluctuations. Right: 1D energy density spectra of the streamwise velocity. The arrow indicates the empirical upper limit of validity of the S&H spectrum according to Adrian and Yao [3].

for higher-order reconstructions using linear and cubic Hermite spline interpolations. With all techniques the original distribution is very well recovered. This is also evident from the corresponding 1D energy density spectra in comparison to reference spectra [33,58]. However, both the linear and cubic Hermite curves show an increased energy roll-off at high frequencies, which could be mistaken as the onset of the dissipation range. The S&H estimate follows the expected $-2/3$ slope slightly longer, but shows an enhanced spectral aliasing effect. As discussed by Adrian and Yao [3], S&H affects the spectrum through additive step-noise caused by the holding mechanism, whose contribution diminishes for high data rates with $\dot{N}^{-3}$ and, secondly, through a low-pass filter with a cut-off frequency at $\dot{N}/(2\pi)$. This designates the upper limit of an unbiased spectral estimate (see arrow in Fig. 7). However, in the low-frequency range, which can be resolved directly with LES, the interpolation techniques provide reliable estimates. Simple S&H performs equally well as linear and cubic reconstructions and was selected as the method of choice in this study due to its robustness and assessable statistical bias [3,70], which is less well-explored for the other approaches [21,53].

3.3 Large-eddy simulation

Turbulence-resolving CFD computations were conducted with the urban aerodynamics LES code FAST3D-CT that is developed and operated by the U.S. Naval Research Laboratory. The model is based on a monotone integrated large-eddy simulation (MILES) methodology [8,11] that handles dynamical effects of sub-grid scales implicitly through numerical diffusion using the flux-corrected transport (FCT) approach [12,13,7,5]. Relevant physics and numerics within FAST3D-CT are discussed in detail by Patnaik et al. [51,50].

3D flow simulations were performed in a 4 km × 4 km computational domain encompassing the inner city of Hamburg (Fig. 2). The computations were conducted on a structured Cartesian grid with a uniform resolution of 2.5 m up to a height of 101.5 m above ground (approx. $3H$; corresponding to the lowest 42 grid cells). From there on the grid was gradually stretched vertically up to the domain top at 1.4 km. Overall the computational domain was covered by $1,600 \times 1,600 \times 80$ grid cells in x, y, z directions.

Buildings were represented by using simple grid masking. In order to avoid very steep vertical gradients at the surface, rolling terrain was represented with a much smoother shaved-cell approach. While the masking procedure is computationally efficient, it leads to a staggering of surfaces ("staircase effects"), for example for slanted roofs or building oriented at oblique angles within the grid. This needs to be kept in mind when comparing local flow features to the wind-tunnel measurements that were conducted in a model of much higher geometric resolution. As in the laboratory model, urban vegetation, bridges, traffic overpasses and passages through buildings or openings to indoor areas were not reproduced.

Turbulent, time-dependent inflow boundary conditions were generated at each time-step by using an imposed fluctuation method. Artificially generated, deterministic turbulent fluctuations are superimposed on mean flow profiles that are based on information from the wind-tunnel approach flow. The non-periodic velocity fluctuations were constructed from a non-linear superposition of different fluctuation wavelengths and amplitudes (see [10,51] for details). At the bottom of the domain a rough-wall boundary layer model is used to represent wall shear stresses. At the domain top and at the lateral boundaries extra layers of cells were implemented to act as a buffer between the self-consistent simulation and the analytically prescribed boundary constraints. Here, an inflow-outflow algorithm is used that changes continuously from the analytical inflow specification described above to a simple extrapolation for an open outflow [10].

The simulation ran for 7 weeks on an SGI Altix computer with 64 CPUs, using a computational time step of 0.05 s at a velocity of approximately 7 m s^{-1} at 200 m above ground. Velocity signals were extracted at cell centres every 0.5 s of real time over a duration of 23,250 s (approx. 6.5 h). The geometric and physical complexity of the model was as close as possible to that of the experiment. As in the laboratory, the mean inflow wind direction was from 235° and the atmospheric stratification was set to neutral. The characteristic flow Reynolds number for the LES was $Re \simeq 1.12 \cdot 10^9$ based on the domain depth of 1.4 km and a velocity of 12 m s^{-1} at that height, whereas Re_H was $9.72 \cdot 10^6$.

The approaching LES boundary-layer flow was compared to the wind-tunnel conditions at the flow reference location above the river upstream of the inner city (site BL04; Fig. 3), allowing enough fetch for the simulation to reach a "self-contained" state. Within the roughness sublayer profiles of mean flow and turbulence statistics were in very good quantitative agreement with the experiment. Comparing energy-density spectra, however, revealed that above $1H$ the artificial inflow turbulence prescribed at the inlet still left a footprint in the flow structure. In particular, this showed in LES spectral energy peaks being located at higher frequencies (i.e. smaller eddies scales) than their wind-tunnel counterparts. Further downstream within and above the city these effects were "washed out", indicating an increase in physical quality of the simulation in response to real obstacle-induced turbulence.

The specific purpose of the simulation with FAST3D-CT was the provision of flow data for the use in the emergency response plume model CT-Analyst, a tool that can be used for fast predictions of the dispersion of air-borne contaminants from localised releases in cities [9,6]. For this purpose the LES data is processed to derive mean-flow statistics and local velocity fluctuation characteristics, from which typical urban dispersion pathways are extrapolated in the lower roughness sublayer (up to an elevation of $2H$). The validation effort, therefore, is focused on determining whether building-induced turbulence and exchange processes are simulated accurately. An in-depth investigation of time series can help to reveal sources of inaccuracy that may not show in low-order statistics (e.g. through error cancellation) and enables a deeper understanding of strengths and limitations of the model, also with a view to other types of applications.

4 Mean flow features

In this section results of the first testing level of the LES validation scheme (Fig. 1) are presented using a fixed Cartesian model coordinate system (x,y,z) as indicated in Fig. 6. The corresponding streamwise, spanwise and vertical components U_i $(i = 1,2,3)$ of the velocity vector are denoted as U, V and W. Overbars denote time-averaged quantities. Velocity statistics are presented in a dimensionless framework based on the mean streamwise reference velocity U_{ref} (Sect. 3.2.2).

Data from the LES were extracted at cell centres and associated with the wind-tunnel measurement points based on a nearest neighbour pairing, i.e. the simulation results were not spatially interpolated to the locations of the wind-tunnel measurements points. This approach can result in horizontal and vertical offsets between the data pairs. These offsets, however, are mostly in the order of the spatial accuracy of the LDA measurement technique, which is dominated by the extent of the measuring volume along its principle axis of 1.6 mm, corresponding to 0.56 m in full scale taking into account the model scale of 1:350 (Sect. 3.2.2). In U–V mode, the principle axis is aligned with the vertical z-axis and in U–W mode with the lateral y-axis. These spatial resolution aspects of the LDA need to be considered particularly in flow regions with strong velocity gradients.

In the following paragraphs and in Sect. 5, only a fraction of the comparison results can be discussed in detail. The results presented here were selected in order to cover a variety of different flow scenarios at sites that were indicative of strengths and limitations of the model. The selection is representative of the overall agreement between experiment and LES.

4.1 Vertical flow profiles

Height profiles of mean flow and turbulence statistics derived from the horizontal velocity components are compared in Fig. 8 at four locations covering different geometry-induced flow scenarios: relatively unobstructed flow just downstream of the river (BL07); flow in a spanwise street canyon oriented at approx. 45° from inflow direction (BL12; canyon width approx. 13.5 m), intersection flow (RM03) and flow channelling through a streamwise canyon (RM07; canyon width approx. 14 m). From the wind-tunnel studies, densely spaced vertical velocity profiles are available covering the roughness sublayer up to approximately $2H$, enabling an application-specific validation of the urban aerodynamics code.

Scatter bars for the wind-tunnel values are based on the reproducibility of experimental flow statistics, assessed through a series of repetition measurements at different heights within the urban boundary layer. For this, vertical velocity profiles were taken repeatedly at two locations: site BL07 for U–V measurements and in the wind-tunnel approach flow for U–W measurements in order to have a better data coverage at low heights. For each measurement location, the run-to-run scatter of flow statistics at different measurement heights was determined. In order to provide a conservative estimate, the reproducibility was then based on the maximum value range determined over all heights for the specific statistical quantity of interest. For $\overline{U}/U_{ref}$ the statistical scatter was found to be ± 0.0185, for $\overline{V}/U_{ref}$ ± 0.0204 and for σ_v^2/U_{ref}^2 ± 0.0027.

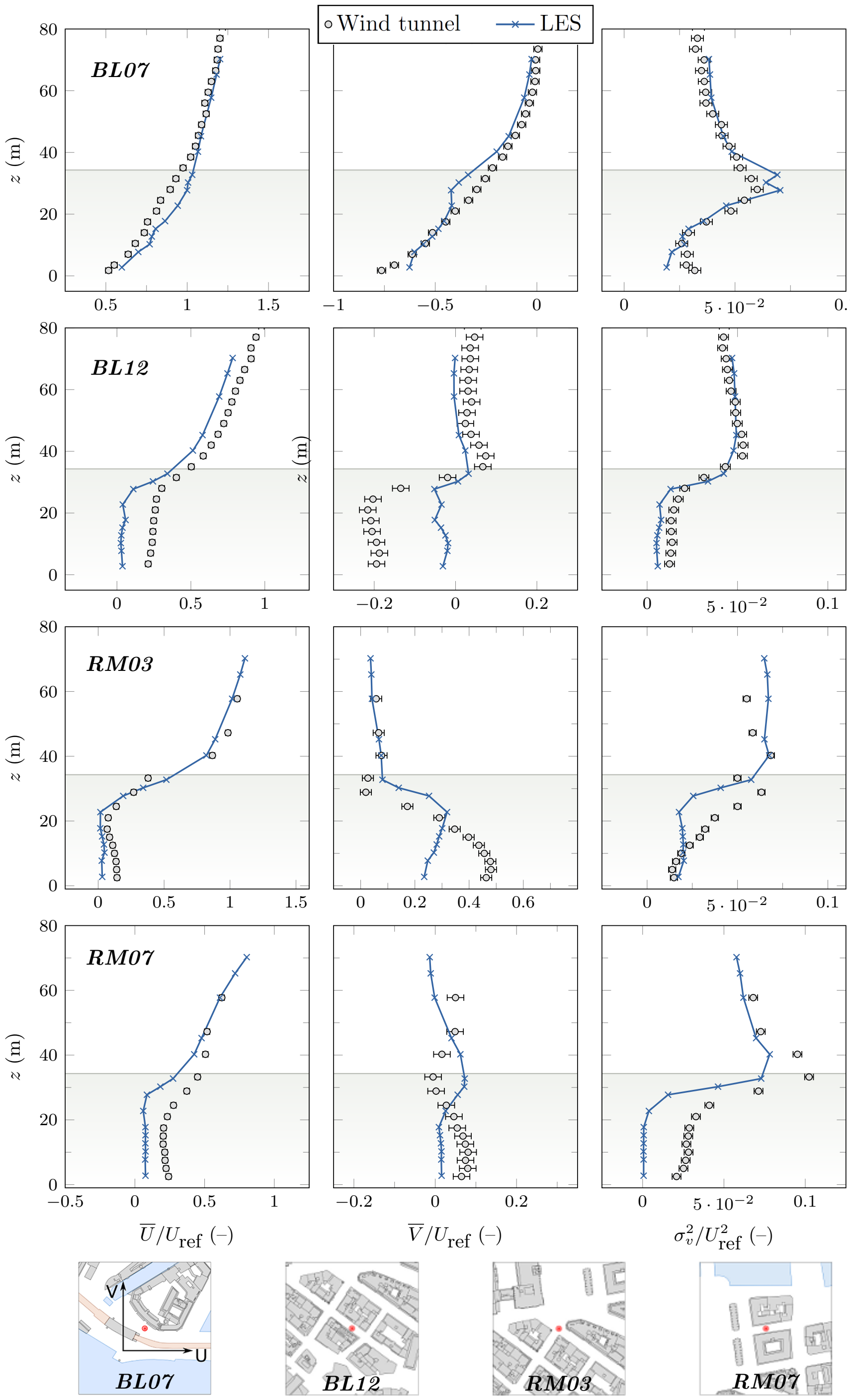

Fig. 8: Comparison of height profiles of means and variances of the horizontal velocity components at different locations within the inner city area (wind tunnel: dots; LES: crosses). The grey shading indicates heights lower than the mean building height of $H = 34.3$ m. Maps showing the location of the comparison points depict an area of 210 m × 210 m.

The results presented here are characteristic for the overall level determined from the entire ensemble of comparison sites. Overall, the LES captures the general qualitative trends of the horizontal mean velocities and variances with height at most of the locations. This, for example, can be seen in the agreement of characteristic peak heights of flow variables at the top of the canopy layer. However, for some of the positions, particularly those characterised by a strong topological confinement of the flow, the quantitative discrepancies are larger for some of the variables compared. Here, the LES shows a systematic trend of under-predicting mean velocities (BL12) and variances (RM07) in the canopy layer. For these two street-canyon locations the ratio of canyon width to LES grid spacing, W/h_i, is of order 5.5. In combination with the "staircase effects" caused by the gridding technique the spatial resolution of 2.5 m in the LES is probably too low to reliably resolve the flow at these points. The relatively coarser representation of buildings in the LES could have caused some of the profile locations to effectively move closer to the building walls, which increases the influence of the prescribed wall-boundary condition on the extracted results.

4.2 Validation metrics

The above comparisons showed that the LES is able to represent, to a reasonable degree, complex urban flow pattern emerging in the roughness sublayer on the mean level at different comparison locations while locally showing trends towards an under-prediction of velocity magnitudes. As recommended for the validation of RANS-based simulations, the exploratory data analysis can be extended into a more quantitative comparison using suitable validation metrics [46, 16]. Fig. 9 depicts scatter plots of wind tunnel against LES results of horizontal velocity statistics, showing overall 135 experimental and numerical data pairs at locations that can be directly compared due to comparatively small spatial offsets. The maximum offset was slightly over 1 m in vertical direction affecting 10 data pairs at the DM site. The majority of scatter points fall well within the margins given by a 1:2 and 2:1 relationship between experiment and simulation. The agreement is further quantified in the next step.

From the large variety of available validation metrics, see e.g. [28, 16, 26], we have selected a choice of the most common methods (Eqs. 1–4) to assess: (1) the overall performance of the model with some robustness to infrequently occurring strong over-predictions or under-predictions (i.e. $FAC2$, although $FAC5$ is routinely considered as well), (2) the tendency of the model to over/under-predict ($MNMB$), (3) the mean absolute error of the simulation (FGE), and (4) the degree of common variation (i.e. trends) in both datasets based on the linear correlation coefficient R.

1. Factor of two:

$$FAC2 = \frac{1}{N}\sum_i F_i \text{ with } F_i = \begin{cases} 1, & \text{if } \frac{1}{2} \leq \frac{P_i}{M_i} \leq 2 \\ 0, & \text{otherwise} \end{cases} \tag{1}$$

2. Modified normalised mean bias:

$$MNMB = \frac{2}{N}\sum_i \left(\frac{P_i - M_i}{P_i + M_i}\right) \tag{2}$$

3. Fractional gross error:

$$FGE = \frac{2}{N}\sum_i \left|\frac{P_i - M_i}{P_i + M_i}\right| \tag{3}$$

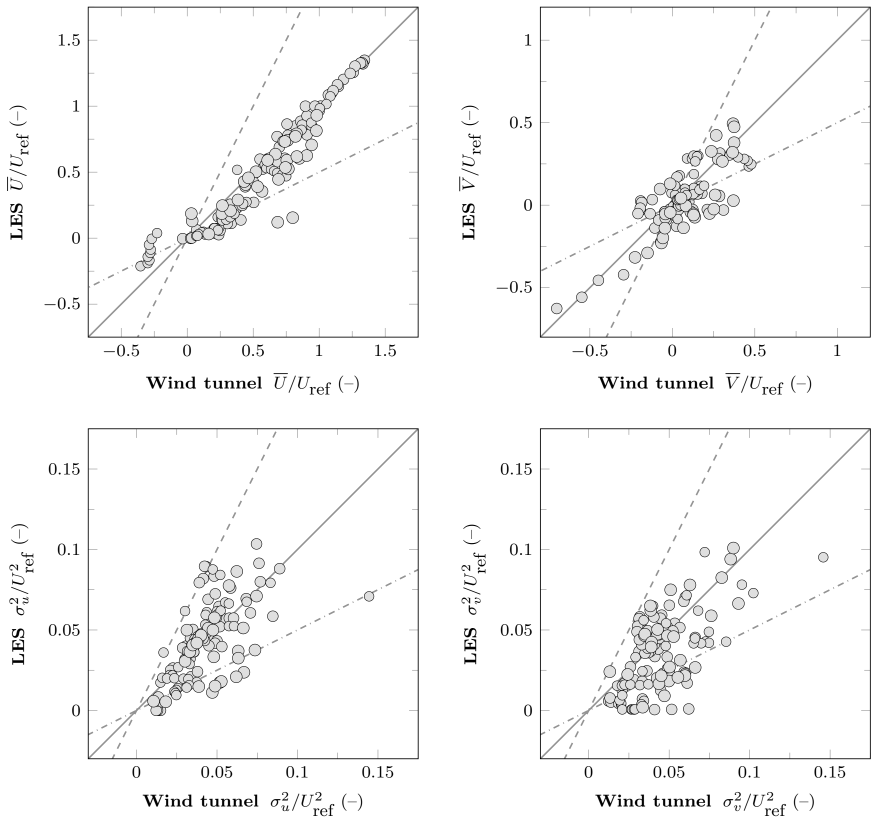

Fig. 9: Scatter plots of wind-tunnel measurements and LES results of horizontal flow statistics $\overline{U}/U_{ref}$, $\overline{V}/U_{ref}$, σ_u^2/U_{ref}^2, and σ_v^2/U_{ref}^2, comprising overall 135 data pairs at 22 comparison sites. Lines indicate the ideal 1:1 relationship and the factor-of-2 margins.

4. Correlation coefficient:

$$R = \frac{\frac{1}{N}\sum_i (P_i - \overline{P})(M_i - \overline{M})}{\sigma_P \sigma_M} \quad (4)$$

Here, P denotes the predicted and M the measured value, and the index $i = 1, \ldots, N$ refers to one of the overall N locations at which statistics are compared. $FAC2$ measures the fraction of LES predictions that are within a factor of two of the corresponding measurement. The simulation bias is assessed by the $MNMB$, which is bounded on the interval $[-2, +2]$. The overall mean error of the simulation can be assessed by the FGE, which is bounded on the interval $[0, +2]$. Both, $MNMB$ and FGE, for which a value of 0 would correspond to a perfect prediction, treat trends of over-predictions and under-predictions symmetrically without over-emphasising outliers. Correlation coefficients, R, are consulted to quantify to whether the same data trends and patterns are seen in the measurements and the LES. In the computation of these validation metrics, the reproducibility of the experimental reference statistics was taken into account as recommended by the COST Action 732 [56].

The validation metrics are presented in Table 1. For all quantities $FAC2$ is above 0.5 indicating that typically more than half of the predictions are within a factor of two of

Table 1: Validation metrics derived for data pairs of horizontal flow statistics (Fig. 9).

	$\overline{U}/U_{ref}$	$\overline{V}/U_{ref}$	$\overline{U_h}/U_{ref}$	σ_u^2/U_{ref}^2	σ_v^2/U_{ref}^2
$FAC2$	0.74	0.52	0.83	0.86	0.77
$MNMB$	-0.40	0.09	-0.28	-0.11	-0.36
FGE	0.44	1.5	0.32	0.32	0.49
R	0.95	0.80	0.94	0.65	0.62

the observations. For dispersion studies in urban areas, this 50% threshold is often recommended for a binary classification of the model skill into sufficient or insufficient, e.g. [28, 18]. More, recently this has been relaxed to 30% in the discussion of acceptance criteria for urban dispersion models by Hanna and Chang [26]. However, these and other studies showed assessments based on single figures of merit should be avoided and further metrics need to be consulted to obtain a clear picture. The negative normalised bias values ($MNMB$) indicate that the LES has a tendency to under-predict. The very good $MNMB$ for $\overline{V}/U_{ref}$, however, is a result of the cancelling of over-predictions and under-predictions, which can be seen very well in the corresponding scatter plot (Fig. 9) in the quite symmetric distribution of values about the 1:1 line at small magnitudes of $\overline{V}/U_{ref}$. Consulting the respective FGE value, which is based on the absolute difference between data pairs, shows that the predictive skill of the model for this velocity component is poor. This was already indicated by the comparatively low $FAC2$ of 0.52. However, comparing the corresponding horizontal wind speeds, $U_h = \sqrt{U^2 + V^2}$, which are independent of the selected coordinate system representation, results in a significantly higher level of agreement than when looking at the velocity components individually. For the other quantities, the FGE indicates a good predictive skill of the LES. The correlation coefficients indicate a high to moderate linear correspondence of data sets. However, the high R value of 0.80 for $\overline{V}/U_{ref}$ clearly is not representative of the actual skill of the code in capturing this component, particularly at flow locations that are characterised by a strong confinement of flow paths as discussed above.

5 Instantaneous flow features

5.1 Frequency distributions

In a next step, frequency distributions of instantaneous horizontal velocities and their corresponding shape and spread parameters are compared.

Fig. 10 shows meteorological wind rose diagrams constructed from wind tunnel and LES time series of instantaneous horizontal wind speeds, U_h, and horizontal directions, U_d, at three heights within a narrow street cross-wind canyon (BL11; W = 17.5 m), together with corresponding vertical profiles. At the first comparison level (z_{exp} = 17.5 m), the wind roses indicate opposing flow channelling directions in the experiment and LES, with the latter significantly under-predicting velocity magnitudes. This is mainly caused by a flawed representation of the V component. The shapes of both distributions, however, are similar in that both exhibit a slight bimodal pattern. Having regard to the narrow width of the canyon, the LES grid resolution seems insufficient to adequately resolve the flow at this site. As discussed above, this problem is reinforced by the gridding technique that can result in a further virtual reduction of the width of the canyon. Hence, in the LES the comparison point can be much closer to the building façade as in the experiment. At the second comparison level

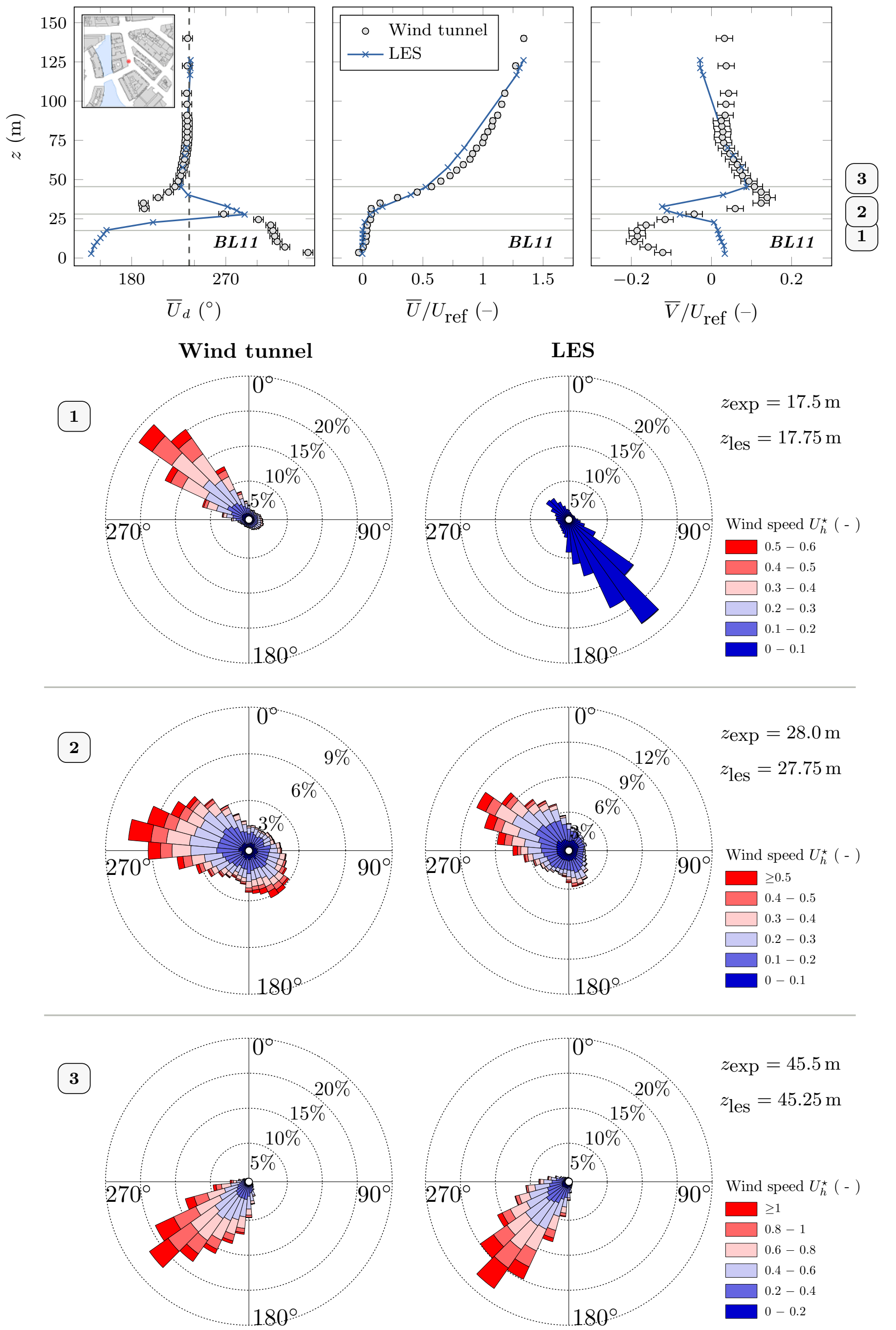

Fig. 10: Wind rose diagrams of the instantaneous horizontal wind speeds U_h/U_{ref} at three heights within and above a narrow street canyon (site BL11) for the wind tunnel (left) and the LES (right). Vertical profiles of the horizontal wind direction, U_d, and both horizontal mean velocities are shown for reference at the top (wind tunnel: dots; LES: crosses).

(z_{exp} = 28 m), this effect is significantly mitigated and the LES performs remarkably well. At this height, the flow path has broadened significantly, as the upstream building is composed as a step-down notch with heights of 40 m and 23 m. Here, the flow is characterised by rather complex recirculating winds, which exhibit two peak directions corresponding to the SE–NW orientation of the canyon. The bimodal nature of the flow is very well reproduced in the LES. At the third comparison height (z_{exp} = 45.5 m) just above the roof-level of the upstream building, both flows have readjusted to the prescribed south-westerly inflow direction, resulting in comparable wind direction distributions.

Fig. 11 shows similar comparisons at different horizontal locations at the entrance into a courtyard (DM site; see Fig. 3). The entrance has a width of 14.5 m width. Horizontal spacings between the comparison locations are in the range of 6 m to 10 m. With heights of 32 m (upper building) and 30 m (lower building) the buildings forming the entrance are slightly lower compared to H. The wind roses are compared at two heights.

At the first comparison level, located at about half the local building height, LES and wind tunnel wind roses at the windward entrance (sites 01–04) are in very good agreement. Within the passage (sites 11–12), flow channelling resulted in higher velocity magnitudes and a narrowing of the frequency distributions compared to the impinging flow. The channelling effect is much stronger in the experiment, where the majority of observed instantaneous wind speeds are in the order of or larger than the reference velocity, U_{ref}, which corresponds to a much higher elevation. The strong width reduction of the LES wind roses goes hand in hand with a tendency towards decreased velocity variances in very narrow street canyons (Fig. 8).

At the second comparison layer, the agreement significantly increases at the windward and leeward passage exits. Within the passage, however, the LES wind roses clearly show a readjustment of the flow to the inflow direction. Here the widths of the distribution are comparable to those of the impinging, unobstructed flow (locations 01–04). This is not evident in the experiment, where the orientation of the wind roses still indicate topological flow channelling. These differences can be explained by the vertical offset of 0.5 m between numerical and experimental data pairs. That close to the local roof-level, where strong vertical velocity gradients have to be expected, such an offset can already have a significant influence on the comparability of the results.

5.2 Shape parameters

The above qualitative analysis of the shape and spread of experimental and LES frequency distributions is supported by a quantitative comparison of high-order statistical moments such as skewness (γ; third moment), quantifying the symmetry of the distribution, and kurtosis (β; fourth moment), measuring its peakedness [69]. For a normally distributed (Gaussian) data sample $\gamma = 0$ and $\beta = 3$. If $\gamma < 0$, the distribution is said to be left-skewed (longer left tail, centre of mass lies to the right). For $\gamma > 0$ the distribution is right-skewed (longer right tail). A leptokurtic distribution with $\beta > 3$ exhibits a higher peak and fatter tails than a Gaussian distribution, while the platykurtic counterpart ($\beta < 3$) is flat-topped with thin tails.

Fig. 12 shows height profiles of γ and β of the streamwise velocity component at four example locations. The parameters were derived from velocity samples for which such high-order statistics are meaningful, i.e. from unimodal distributions that further do not exhibit plateaus or extremely heavy tails. The scatter bars attached to the measurement data were derived from repetition measurements yielding a maximum range of ± 0.146 for γ and ± 0.203 for β. For the majority of points, the LES shape parameters fall well within the scatter of the

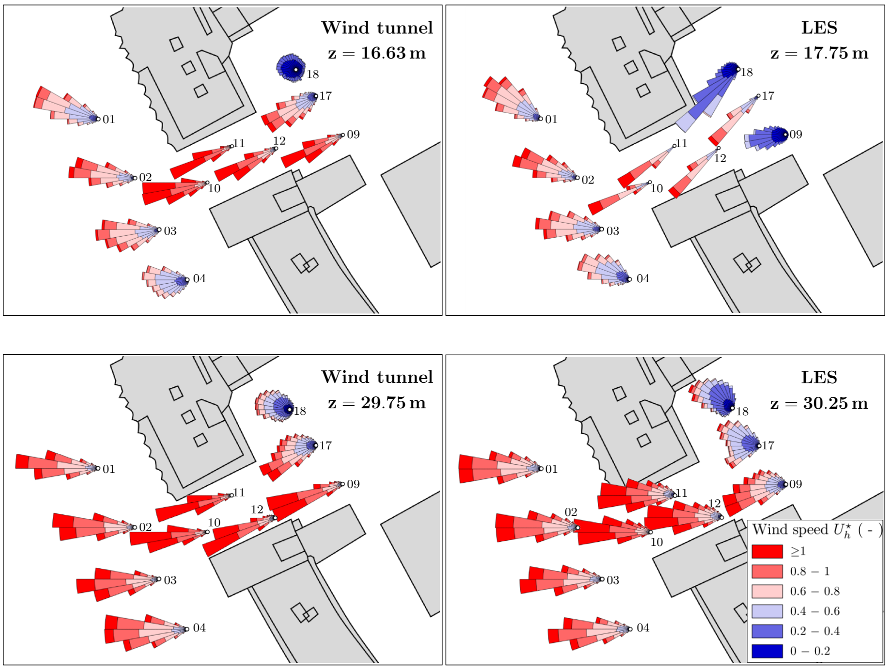

Fig. 11: Wind rose diagrams of wind tunnel (left) and LES (right) instantaneous horizontal wind speeds and directions at half the mean building height (approx. $0.5H$; top) and just below the mean building height (approx. $0.9H$; bottom) at the DM site. Note that the positions of the wind roses are not true to the exact (x,y) locations of the data points, but are shifted for a clearer display (see Fig. 3 for the exact locations). For the same reason, the percentage circles of the wind direction bars are omitted, but the same percentage range has been used in both cases. The map dimension is 90 m × 70 m. The flow is approaching from the left.

wind-tunnel equivalents. This statement holds for the rather unobstructed wind field above the Elbe river (BL04), but at comparison points further downstream within the inner city. The distinct vertical variability of skewness and kurtosis found at the intersection location BL10 is very well reproduced in the LES, which is an indication that the code is able to capture the flow structure at this site rather well.

Fig. 13 shows scatter plots of LES and wind tunnel high-order statistics derived from distributions of the instantaneous velocities U and V at the sub-sample of sites that where unimodal distributions were found. The majority of analysed LES and wind tunnel velocity signals exhibit more or less Gaussian shape characteristics. However, the scatter plots for γ reveal that there is a tendency towards a positive skewness of the U/U_{ref} signals (i.e. a trend toward tails at high velocities) in the experiment, while for the spanwise components, V/U_{ref}, more distributions are skewed to the left (tails at low velocities). These patterns are also seen in the LES. Offsets between the shape descriptors are more distinct for V/U_{ref}. More acute peaks and shorter tails ($\beta > 3$), for example, are observed in some of the LES velocity distributions. This trend of more leptokurtic LES velocities has been addressed in the

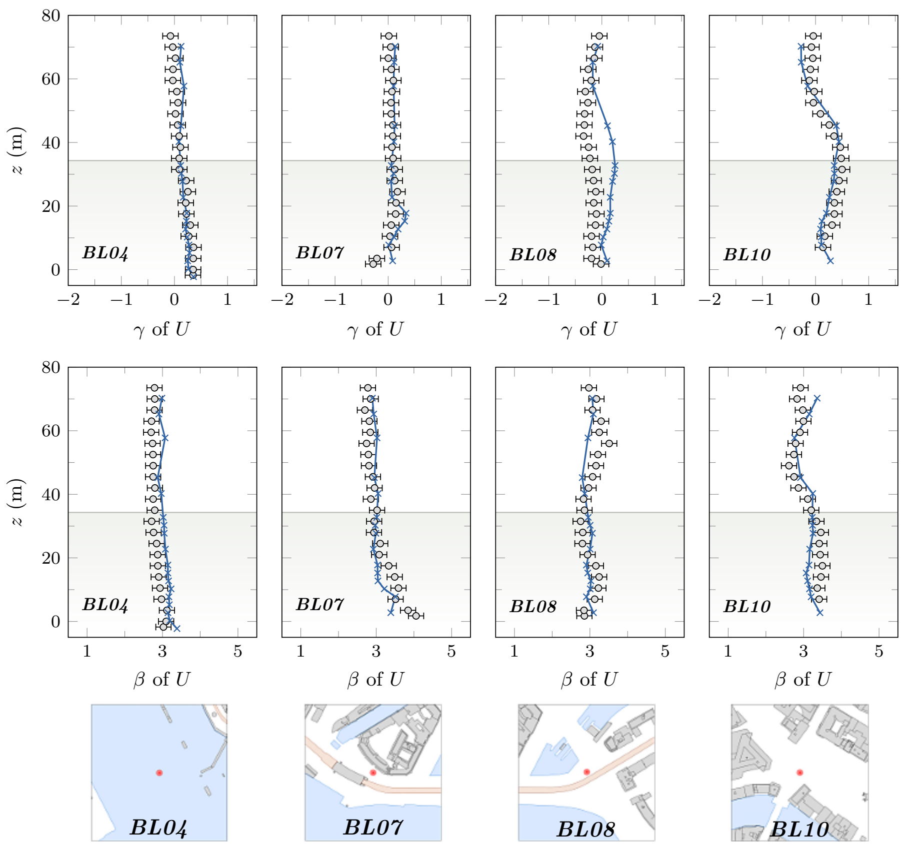

Fig. 12: Wind tunnel (dots) and LES (crosses) height profiles of skewness, γ (top), and kurtosis, β (bottom), of the streamwise velocity component at four sites. Heights below H are indicted by a grey shading.

previous section and is associated with physical and geometrical resolution characteristics in geometrically confined situations.

5.2.1 Wind direction fluctuations

In order to compare the time-dependency of statistical characteristics, we derive fluctuation time scales of the horizontal wind vector. Such an analysis is targeted at the quantification of typical time scales associated with a certain shift of the horizontal wind vector, which can be measured by direction differences as a function of time lag.

Results are presented for location BL04 above the Elbe river. Here the prevailing wind direction approximately agrees with the approach flow wind direction. Fluctuations of the horizontal wind direction are defined as $u'_d(t) = U_d(t) - \overline{U}_d$. Fig. 14 depicts frequency distributions of u'_d at four heights. The distributions reveal that the value range of the wind direction fluctuations is gradually narrowing with increasing distance from the ground as the distributions tend to become more peaked. Comparable height trends are present in both

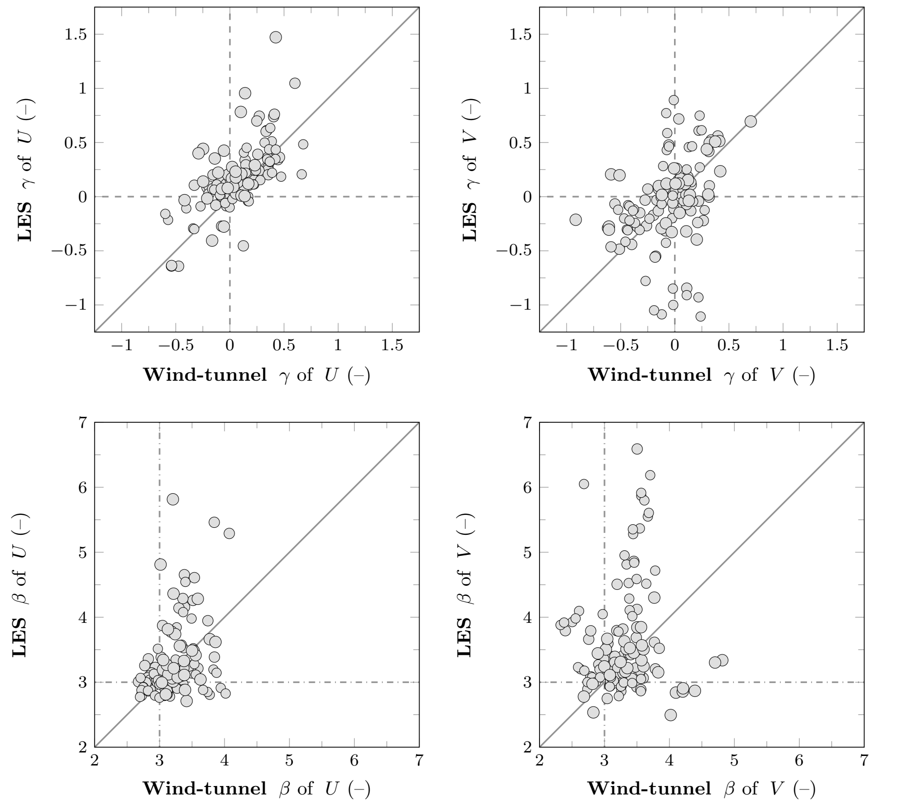

Fig. 13: Scatter plots of wind tunnel versus LES skewness, γ, and kurtosis, β, of the horizontal velocity components. Dashed lines indicate the Gaussian limits of $\gamma = 0$ and $\beta = 3$, while the solid line shows the 1:1 relationship.

data sets and there is a high level of agreement between spread and shape characteristics of experimental and LES distributions. This indicates that the latter is capturing the transition between the stronger influence of smaller/short-lived eddies near the ground (high turbulence intensities) to larger/long-lived structures well above ground (low turbulence intensities).

Absolute differences of horizontal wind directions as a function of time lag, $|\delta U_d(t_l)|$, are compared in a next step (Fig. 15) as an indicator for the fluctuation intensity of the wind vector in the horizontal plane, which is essentially coupled to the structure of the flow. The evaluation is based on the median differences in order to account for the fact that the distributions tend to be strongly right-tailed. As a measure of observed value spread, the interquartile range (IQR) of the distributions (difference between the 75th and 25th percentile) is given as well. For this analysis, resampled (equally spaced) wind-tunnel time series were analysed (see Sect. 3.2.3). The time lag is defined as $t_l = n f^{-1}$, with $n = 0, \ldots, N/2$ and N being the number of signals in the time series. The frequency, f, either refers to the sampling frequency of the LES, f_s, or to the mean data rate of the experiment, $\dot{N}$. Hence, while the time lags are the same at all heights in the LES since $f_s = const$, point-to-point differences are present for the experimental data because $\dot{N}$ is location dependent. Fig. 15 shows results

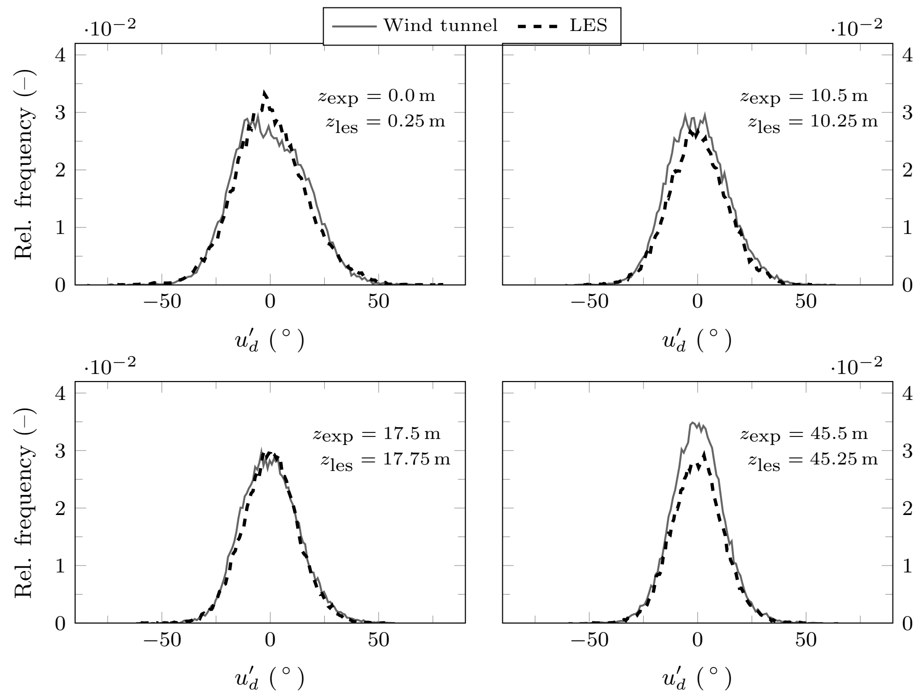

Fig. 14: Relative frequency distributions of horizontal wind direction fluctuations, u'_d, about the local time-average, $\overline{U}_d$, in the experiment (solid lines) and the LES (dashed lines) at four heights above the Elbe river (BL04). Note that the z-axis is defined with reference to ground level, to which the water level is vertically offset by -3.5 m.

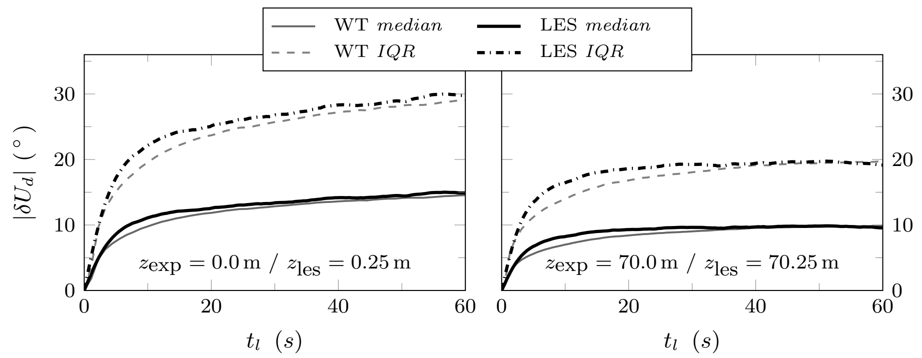

Fig. 15: Median absolute wind direction differences (wind tunnel: solid lines; LES: thick solid lines) together with the corresponding interquartile range (IQR; wind tunnel: dashed lines; LES: dash-dotted lines) as a function of full-scale time lag for a reference velocity of $U_{ref} = 5$ m s^{-1}. The wind tunnel (WT) and LES data are displayed for two heights above the Elbe river (BL04).

for two heights above the river (BL04). The time lags are displayed in full-scale dimension, using a reference wind speed of $U_{ref} = 5$ m s^{-1} for scaling. A high level of agreement between both data sets is found for the measures of central tendency and spread. The LES is able to reproduce the experimental statistics on a point-by-point basis, but also with respect to the overall time-development of the wind-angle differences as a function of height. At both heights a relatively strong increase in the observed wind direction differences over the first 10 s or so is followed by a pronounced flattening of the curves with a later levelling-off into a plateau. The curves reveal a distinct height dependency, showing clearly as a decrease with height of the median wind direction differences at the maximum displayed time lag of $t_l = 60$ s. This decrease is accompanied by a reduction of the spread of the underlying distributions, in agreement with above results from the comparison of direction fluctuations. The magnitude of the IQRs emphasise the variability in the angle-difference samples for a specified time lag. Even for small temporal offsets, the wind direction shifts can become quite large due to the strong turbulent variability of the flow near the surface. This indicates how low-frequency oscillations of the wind vector in the horizontal plane associated with larger-scale eddies (longer time lags) are superimposed by high-frequency fluctuations, which are stronger near the ground. The only systematic differences noticeable in the results shown in Fig. 15 are seen in the slopes of the LES curves at small time lags, which are slightly higher than their wind-tunnel counterparts, but then tend to level off faster.

6 Discussion and conclusions

This study aims to identify and test a strategy for an in-depth validation of eddy-resolving simulations for turbulent flow in the near-surface atmospheric boundary layer. We propose a three-level comparison procedure and test its applicability based on the example of urban flow simulated with an implicit LES code. Detailed wind-tunnel measurements within a realistic urban scale model provide the reference data.

6.1 Suitability of the reference experiment

It is necessary to confirm first that the reference experiment is suitable for a meaningful and fair comparison with the simulation. The proposed validation strategy puts a strong emphasis on the analysis of time series for the comparison of flow structures. Hence the experimental data have to be of suitable quality for advanced signal processing and it has to be verified that the laboratory measurements fulfil specific quality requirements. This concerns the representativeness of the wind-tunnel model for the physical problem of interest (similarity requirements), the qualification of the measured velocity data for advanced signal processing (signal quality and resolution properties), and the statistical robustness of derived quantities (experimental reproducibility). For the test scenario covered in this study the following was ensured:

– Geometric and dynamic similarity requirements are met by the experiment
– Inflow conditions comply with field observations and established standards for the physical modelling of turbulent boundary layers
– Signal durations are long enough to minimise the inherent uncertainty of derived statistics and to perform a statistically representative analysis of large eddies in the flow (this can be experimentally verified through temporal convergence tests of statistical quantities)

– Sampling frequencies are high enough to capture turbulence structures that are directly resolved with LES
– The statistical reproducibility of experimental results, e.g. as derived from repetition measurements, is documented
– The bias resulting from the resampling of LDA signals is quantifiable and minimised

Similar requirements regarding the quality and level of documentation of data and boundary conditions of the experiment also apply to reference measurements carried out in the field. Due to the natural variability of the atmosphere it is essential that the ambient meteorological conditions over the course of the field campaign are well documented at representative locations in order to define the boundary conditions for the simulation [37]. In complex environments like cities, it is also essential that sensor sites are characterised in detail, e.g. regarding the local urban structure, surface cover or anthropogenic factors [48].

6.2 Exploratory data analysis

By applying the first level of the validation concept to the Hamburg test case we were able to identify general features of the simulation in terms of mean flow and turbulence statistics in comparison to the experiment at topologically different locations within the city. With the analysis of frequency distributions the scene was set for a more in-depth comparison of physical information hidden deeper within the time series.

Mean flow characteristics With this “traditional” comparison of mean flow and turbulence statistics, typical obstacle-induced flow scenarios like recirculation zones, channelling effects or strong lateral flow deflections at street-level can be investigated. This type of analysis provides a valuable initial overview about how LES and experiment compare and is helpful to identify cases of strong agreement or disagreement. The accuracy of the statistics can be quantified by using sets of validation metrics, possibly in combination with established quality acceptance thresholds. Discrepancies between LES and experiment should be evaluated on a point-by-point basis. In this study, systematic quantitative differences were determined, with the LES having a tendency to under-predict velocity magnitudes within the UCL. This mostly affects locations where the flow path is strongly confined by surrounding buildings. Depending on the alignment of the buildings within the numerical grid, some LES sites are located closer to solid boundaries than in the wind tunnel as a result of the comparatively coarse obstacle representation through the blocking of entire grid cells. Another factor affecting the comparability are spatial offsets between the wind tunnel and LES data locations. Interpolating the LES data from the 2.5 m grid is not expected to mitigate this issue in regions of strong velocity gradients. Here, spatial resolution properties of the experimental data also have to be considered. For the test case, these are primarily determined by the length of the LDA measuring volume (0.56 m full-scale). Such resolution and siting aspects need to be considered when dealing with highly three-dimensional, obstacle-induced turbulence.

Velocity sample characteristics From the mean flow analysis alone no definite conclusions about the agreement of the underlying data samples can or should be drawn; all information available in the time series is condensed into single parameters. By exploring the value range or occurrence probabilities of predicted quantities key reasons emerge to prefer time-resolved methods over significantly less expensive steady-state RANS alternatives. A simple yet rarely pursued way to extend the exploratory assessment of a model's predictive skill is to focus on frequency distributions of velocities and derived quantities. Particularly in cases where LES is not only intended to deliver reliable statistics, but also expected to give an accurate account of the value range that can be expected (e.g. with regard to extreme values) the comparison of frequency distributions is essential. The occurrence of bimodal and heavy-tailed velocity distributions is anything but rare in urban environments and should be reproducible by eddy-resolving models. Comparisons of velocity and wind direction histograms for the Hamburg test scenario showed that the LES captures complex geometry-induced flow patterns realistically. In order to quantify this agreement, higher-order distribution shape measures should be directly compared. For the case of unimodal distributions, skewness and kurtosis parameters showed a very good agreement of associated height profiles at comparison points sufficiently far away from building façades. The analysis of time scales and distributions of wind vector fluctuations in the horizontal plane can provide additional information about the scales of eddies associated with shifts in wind direction.

6.3 Outlook

With the concluding analysis of wind vector time scales, the study advanced towards an important aspect of the LES validation problem: the comparison of time-related turbulence statistics that are indicative of eddy structures in the flow. LES is expected to directly resolve the energy and flux-dominating turbulent eddies. Within urban areas, the size of the largest eddies is restricted by the geometry and hence smaller than for example in the outer regions of the surface layer. Hence it needs to be carefully evaluated whether the chosen grid resolution (2.5 m in this case) is sufficient to represent UCL turbulence accurately. The conclusions drawn about the agreement of mean flow and turbulence statistics should be re-evaluated in light of the accuracy with which eddy scales are represented in the LES. Comparing statistics associated with dominant scales of motion provides valuable insight into the quality of the simulation. This is focused on in part II of the study by advancing the "testing level" to the next stage by: (i) comparing turbulence features through an analysis of integral time scales and energy density spectra; (ii) analysing the structure of the flow with conditional resampling as part of the quadrant analysis of the vertical turbulent momentum transfer and by using a wavelet transform method to compare the time-frequency content of LES and laboratory flow.

Acknowledgements The numerical simulations with the LES code FAST3D-CT were carried out at the Laboratories for Computational Physics and Fluid Dynamics of the U.S. Naval Research Laboratory in Washington D.C., USA. The authors wish to express their thanks to Jay Boris, Mi-Young Obenschain and other collaborators there. Further thanks is given to colleagues at the Environmental Wind Tunnel Laboratory at the University of Hamburg. Financial funding by the German Federal Office of Civil Protection and Disaster Assistance as well as by the Ministry of the Interior of the City of Hamburg within the "Hamburg Pilot Project" is gratefully acknowledged (BBK research contract no. BBK III.1-413-10-364). Parts of the wind-tunnel model construction were financially supported by the KlimaCampus at the University of Hamburg.

References

1. Guide for the Verification and Validation of Computational Fluid Dynamics Simulations (AIAA G-077-1998(2002)). American Institute of Aeronautics and Astronautics, Inc. DOI doi:10.2514/4.472855.001
2. Adrian, R.J., Meneveau, C., Moser, R.D., Riley, J.: Final report on 'Turbulence Measurements for LES' workshop. Tech. rep., Department of Theoretical and Applied Mechanics, University of Illinois at Urbana-Champaign, Urbana (IL), USA (2000)

3. Adrian, R.J., Yao, C.S.: Power spectra of fluid velocities measured by laser Doppler velocimetry. Exp Fluids **5**, 17–28 (1987)
4. ASME: Guide for verification and validation in computational solid mechanics. ASME V&V 10-2006, The American Society of Mechanical Engineers, New York (NY), USA (2006)
5. Book, D.L.: The conception, gestation, birth, and infancy of FCT. In: D. Kuzmin, R. Löhner, S. Turek (eds.) Flux-Corrected Transport: Principles, Algorithms, and Applications, Scientific Computing, second edn., pp. 1–21. Springer (2012)
6. Boris, J., Patnaik, G., Obenschain, K.: The how and why of Nomografs for CT-Analyst. Report NRL/MR/6440-11-9326, Naval Research Laboratory, Washington (DC), USA (2011)
7. Boris, J.P.: New directions in computational fluid dynamics. Annu Rev Fluid Mech **21**, 345–385 (1989)
8. Boris, J.P.: On large eddy simulation using subgrid turbulence models. In: J.L. Lumley (ed.) Whither Turbulence? Turbulence at the Crossroads, *Lecture Notes in Physics*, vol. 357, pp. 344–353. Springer (1990)
9. Boris, J.P.: The threat of chemical and biological terrorism: Preparing a response. Comput Sci Eng **4**, 22–32 (2002)
10. Boris, J.P.: Dust in the wind: Challenges for urban aerodynamics. AIAA Paper 2005-5393 (2005)
11. Boris, J.P.: More for LES: A brief historical perspective of MILES. In: F.F. Grinstein, L.G. Margolin, W.J. Rider (eds.) Implicit Large Eddy Simulation: Computing Turbulent Fluid Dynamics, pp. 9–38. Cambridge University Press (2007)
12. Boris, J.P., Book, D.L.: Flux-corrected transport I: SHASTA – A fluid transport algorithm that works. J Comput Phys **11**, 38–69 (1973)
13. Boris, J.P., Book, D.L.: Solution of the continuity equation by the method of flux-corrected transport. In: B. Alder, S. Fernbach, M. Rotenberg, J. Killeen (eds.) Methods in Computational Physics, vol. 16, pp. 85–129. Academic Press (1976)
14. Bradshaw, P.: The understanding and prediction of turbulent flow. Aeronaut J **76**, 403–418 (1972)
15. Britter, R., Schatzmann, M. (eds.): Background and justification document to support the model evaluation guidance and protocol. COST Action 732. University of Hamburg, Germany (2007a)
16. Britter, R., Schatzmann, M. (eds.): Model evaluation guidance and protocol document. COST Action 732. University of Hamburg, Germany (2007b)
17. Britter, R.E., Hanna, S.R.: Flow and dispersion in urban areas. Annu Rev Fluid Mech **35**, 469–496 (2003)
18. Chang, J.C., Hanna, S.R.: Air quality model performance evaluation. Meteorol Atmos Phys **87**, 167–196 (2004)
19. Cheng, W.C., Liu, C.H.: Large-eddy simulation of turbulent transports in urban street canyons in different thermal stabilities. J Wind Eng Ind Aerod **99**, 434–442 (2011)
20. Counihan, J.: Adiabatic atmospheric boundary layers: A review and analysis of data from the period 1880 - 1972. Atmos Environ **9**, 871–905 (1975)
21. De Waele, S., Broersen, P.M.T.: Error measures for resampled irregular data. IEEE T Instrum Meas **49**, 216–222 (2000)
22. Edwards, R.V., Jensen, A.S.: Particle-sampling statistics in laser anemometers: sample-and-hold systems and saturable systems. J Fluid Mech **133**, 397–411 (1983)
23. ESDU: Characteristics of atmospheric turbulence near the ground. Part II: single point data for strong winds (neutral atmosphere). ESDU 85020, Engineering Sciences Data Unit, London, UK (1985)
24. Grimmond, C.S.B., Oke, T.R.: Aerodynamic properties of urban areas derived from analysis of surface form. J Appl Meteorol **38**, 1262–1292 (1999)
25. Grinstein, F.F.: Verification and validation of CFD based turbulent flow experiments. In: Encyclopedia of Aerospace Engineering, pp. 515–523. John Wiley & Sons (2010)
26. Hanna, S., Chang, J.: Acceptance criteria for urban dispersion model evaluation. Meteorol Atmos Phys **116**(3), 133–146 (2012)
27. Hanna, S.R., Brown, M.J., Camelli, F.E., Chan, S.T., Coirier, W.J., Kim, S., Hansen, O.R., Huber, A.H., Reynolds, R.M.: Detailed simulations of atmospheric flow and dispersion in downtown manhattan: An application of five computational fluid dynamics models. B Am Meteorol Soc **87**(12), 1713–1726 (2006)
28. Hanna, S.R., Hansen, O.R., Dharmavaram, S.: FLACS CFD air quality model performance evaluation with Kit Fox, MUST, Prairie Grass, and EMU observations. Atmos Environ **38**, 4675–4687 (2004)
29. Hertwig, D.: On Aspects of Large-Eddy Simulation Validation for Near-Surface Atmospheric Flows. Ph.D. thesis, Universität Hamburg (2013). URL http://ediss.sub.uni-hamburg.de/volltexte/2013/6289/pdf/Dissertation.pdf
30. Hertwig, D., Efthimiou, G.C., Bartzis, J.G., Leitl, B.: CFD-RANS model validation of turbulent flow in a semi-idealized urban canopy. J Wind Eng Ind Aerod **111**, 61–72 (2012)
31. Hertwig, D., Leitl, B., Schatzmann, M.: Organized turbulent structures – Link between experimental data and LES. J Wind Eng Ind Aerod **99**, 296–307 (2011)

32. Huang, H., Ooka, R., Kato, S.: Urban thermal environment measurements and numerical simulation for an actual complex urban area covering a large district heating and cooling system in summer. Atmos Environ **39**(34), 6362–6375 (2005)
33. Kaimal, J.C., Wyngaard, J.C., Izumi, Y., Coté, O.R.: Spectral characteristics of surface-layer turbulence. Q J Roy Meteor Soc **98**, 563–589 (1972)
34. Kanda, M.: Progress in urban meteorology: A review. J Meteorol Soc Jpn Ser. II **85B**, 363–383 (2007)
35. Kempf, A.M.: LES validation from experiments. Flow Turbul Combust **80**, 351–373 (2008)
36. Konow, H.: Tall Wind Profiles in Heterogeneous Terrain. Ph.D. thesis, Universität Hamburg (2015). URL http://ediss.sub.uni-hamburg.de/volltexte/2015/7202/pdf/Dissertation.pdf
37. Leitl, B.: Validation data for microscale dispersion modelling. EUROTRAC Newsletter **22**, 28–32 (2000)
38. Li, X.X., Britter, R.E., Koh, T.Y., Norford, L.K., Liu, C.H., Entekhabi, D., Leung, D.Y.C.: Large-eddy simulation of flow and pollutant transport in urban street canyons with ground heating. Bound-Lay Meteorol **137**, 187–204 (2010)
39. Li, X.X., Britter, R.E., Norford, L.K., Koh, T.Y., Entekhabi, D.: Flow and pollutant transport in urban street canyons of different aspect ratios with ground heating: Large-eddy simulation. Bound-Lay Meteorol **142**, 289–304 (2012)
40. Li, X.X., Liu, C.H., Leung, D.Y.C., Lam, K.M.: Recent progress in CFD modelling of wind field and pollutant transport in street canyons. Atmos Environ **40**, 5640–5658 (2006)
41. Liu, Y.S., Cui, G.X., Wang, Z.S., Zhang, Z.S.: Large eddy simulation of wind field and pollutant dispersion in downtown Macao. Atmos Environ **45**, 2849–2859 (2011)
42. Mochida, A., Lun, I.: Prediction of wind environment and thermal comfort at pedestrian level in urban area. J Wind Eng Ind Aerod **96**, 1498–1527 (2008)
43. Moonen, P., Defraeye, T., Dorer, V., Blocken, B., Carmeliet, J.: Urban physics: Effect of the micro-climate on comfort, health and energy demand. Front Archit Res **1**, 197–228 (2012)
44. Moonen, P., Gromke, C., Dorer, V.: Performance assessment of large eddy simulation (LES) for modeling dispersion in an urban street canyon with tree planting. Atmos Environ **75**, 66–76 (2013)
45. Murakami, S., Ooka, R., Mochida, A., Yoshida, S., Kim, S.: CFD analysis of wind climate from human scale to urban scale. J Wind Eng Ind Aerod **81**, 57–81 (1999)
46. Oberkampf, W.L., Barone, M.F.: Measures of agreement between computation and experiment: Validation metrics. J Comput Phys **217**, 5–36 (2006)
47. Oberkampf, W.L., Trucano, T.G.: Verification and validation in computational fluid dynamics. Prog Aerosp Sci **38**, 209–272 (2002)
48. Oke, T.R.: Siting and exposure of meteorological instruments at urban sites. In: C. Borrego, A.L. Norman (eds.) Air Pollution Modeling and its Application XVII, chap. 66, pp. 615–631. Springer (2007)
49. Park, S.B., Baik, J.J., Raasch, S., Letzel, M.O.: A large-eddy simulation study of thermal effects on turbulent flow and dispersion in and above a street canyon. J Appl Meteorol Climatol **51**, 829–841 (2012)
50. Patnaik, G., Boris, J.P., Grinstein, F.F., Iselin, J.P., Hertwig, D.: Large scale urban simulations with FCT. In: D. Kuzmin, R. Löhner, S. Turek (eds.) Flux-Corrected Transport: Principles, Algorithms, and Applications, Scientific Computing, second edn., pp. 91–117. Springer (2012)
51. Patnaik, G., Grinstein, F.F., Boris, J.P., Young, T.R., Parmhed, O.: Large-scale urban simulations. In: F.F. Grinstein, L.G. Margolin, W.J. Rider (eds.) Implicit Large Eddy Simulation: Computing Turbulent Fluid Dynamics. Cambridge University Press (2007)
52. Plate, E.J.: Methods of investigating urban wind fields – physical models. Atmos Environ **33**, 3981–3989 (1999)
53. Ramond, A., Millan, P.: Measurements and treatment of LDA signals, comparison with hot-wire signals. Exp Fluids **28**, 58–63 (2000)
54. Salim, S.M., Buccolieri, R., Chan, A., Di Sabatino, S.: Numerical simulation of atmospheric pollutant dispersion in an urban street canyon: Comparison between RANS and LES. J Wind Eng Ind Aerod **99**, 103–113 (2011)
55. Schatzmann, M., Leitl, B.: Validation of urban flow and dispersion CFD models. In: Proceedings of the 5th International Symposium on Computational Wind Engineering. Chapel Hill, North Carolina (2010)
56. Schatzmann, M., Olesen, H., Franke, J. (eds.): COST 732 model evaluation case studies: Approaches and results. COST Action 732. University of Hamburg, Germany (2010). ISBN 3-00-018312-4
57. Schlünzen, K.H.: On the validation of high-resolution atmospheric mesoscale models. J Wind Eng Ind Aerod **67/68**, 479–492 (1997)
58. Simiu, E., Scanlan, R.H.: Wind Effects on Structures, 2nd edn. John Wiley & Sons, New Jersey (1986)
59. Standen, N.M.: A spire array for generating thick turbulent shear layers for natural wind simulation in wind tunnels. Report LTR-LA-94, National Aeronautical Establishment, Canada (1972)
60. Stathopoulos, T.: Pedestrian level winds and outdoor human comfort. J Wind Eng Ind Aerod **94**, 769–780 (2006)

61. Tamura, T.: Towards practical use of LES in wind engineering. J Wind Eng Ind Aerod **96**, 1451–1471 (2008)
62. Tominaga, Y., Mochida, A., Yoshie, R., Kataoka, H., Nozu, T., Yoshikawa, M., Shirasawa, T.: AIJ guidelines for practical applications of CFD to pedestrian wind environment around buildings. J Wind Eng Ind Aerod **96**, 1749–1761 (2008)
63. Tominaga, Y., Stathopoulos, T.: CFD modeling of pollution dispersion in a street canyon: Comparison between LES and RANS. J Wind Eng Ind Aerod **99**, 340–348 (2011)
64. Tominaga, Y., Stathopoulos, T.: CFD modeling of pollution dispersion in building array: Evaluation of turbulent scalar flux modeling in RANS model using LES results. J Wind Eng Ind Aerod **104-106**, 484–491 (2012)
65. Tominaga, Y., Stathopoulos, T.: CFD simulation of near-field pollutant dispersion in the urban environment: A review of current modeling techniques. Atmos Environ **79**, 716–730 (2013)
66. VDI: Environmental meteorology – Physical modelling of flow and dispersion processes in the atmospheric boundary layer – Application of wind tunnels. Guideline VDI-3783-12, Verein Deutscher Ingenieure (The Association of German Engineers), Beuth Verlag, Berlin (2000)
67. VDI: Environmental meteorology – Prognostic microscale wind field models – Evaluation for flow around buildings and obstacles. Guideline VDI-3783-9, Verein Deutscher Ingenieure (The Association of German Engineers), Beuth Verlag, Berlin (2005)
68. Wettermast Hamburg, Universität Hamburg: URL http://www.wettermast-hamburg.zmaw.de
69. Wilks, D.S.: Statistical Methods in the Atmospheric Sciences, 2nd edn. Academic Press, Waltham (MA) (2005)
70. Winter, A.R., Graham, L.J.W., Bremhorst, K.: Effects of time scales on velocity bias in LDA measurements using sample and hold processing. Exp Fluids **11**, 147–152 (1991)
71. Wyngaard, J.C., Peltier, L.J.: Experimental micrometeorology in an era of turbulence simulation. Bound-Lay Meteorol **78**, 71–86 (1996)
72. Xie, Z.T., Castro, I.P.: LES and RANS for turbulent flow over arrays of wall-mounted obstacles. Flow Turbul Combust **76**, 291–312 (2006)
73. Xie, Z.T., Castro, I.P.: Large-eddy simulation for flow and dispersion in urban streets. Atmos Environ **43**, 2174–2185 (2009)
74. Xie, Z.T., Hayden, P., Wood, C.: Large-eddy simulation of approaching-flow stratification on dispersion over arrays of buildings. Atmos Environ **71**, 64–74 (2013)